GEOPHYSICS, VOL. 78, NO. 6 (NOVEMBER-DECEMBER 2013); P. EN107–EN116, 9 FIGS., 1 TABLE.
10.1190/GEO2013-0099.1

Imaging scatterers in landfills using seismic interferometry

Laura Amalia Konstantaki[1], Deyan Draganov[2], Timo Heimovaara[1], and Ranajit Ghose[2]

ABSTRACT

A significant problem with landfills is their aftercare period. A landfill is considered to be safe for the environment only after a relatively long period of time. Until it reaches such a condition, it has to be periodically treated. Not only are treatments very expensive, but they could be dangerous as well; for example, when barriers limiting the waste break. So far, there is no established technique that can predict the leachate and gas-emission potential of a landfill, especially in time-lapse monitoring. This potential depends on the channeling of fluids due to the presence of high-density waste areas and the redistribution of the channels with time. We propose to use seismic interferometry (SI) applied to active reflection seismics to help improve the image of the waste areas (scatterers) and to monitor the subsurface changes in time. Normally, application of SI to reflection recordings from active sources at the surface would result in an erroneous retrieved result, but secondary illumination of the receivers from strongly scattering subsurface, like a landfill, would remedy this problem. We conduct modeling studies to examine the possible benefits of this approach compared to using the conventional seismic reflection method. We show that the reflections retrieved from SI can be used to obtain a clearer image of the shallower scatterers. In addition, we illustrate that time-lapse monitoring using reflections retrieved by SI shows a more repeatable result than the conventional approach in case of source nonrepeatability.

INTRODUCTION

Government organizations have been dealing with problems caused by municipal solid-waste landfills (MSW, i.e., household waste landfills) over the last decades. Currently, research focuses on the development of treatment methods of MSW to reduce the aftercare period of the landfill (Scharff, 2005; Van Vossen, 2010). The main problems caused by the landfills are uncontrolled emission of leachate (liquid produced from chemical reactions in the waste) and gas (mainly methane and carbon dioxide). For treatment of the landfill, recirculation of leachate or water and aeration or subtraction of oxygen enhances the biological degradation occurring inside the landfill, which leads to faster stabilization and potentially to a shorter after-care period.

Often, the landfill has been treated as a bioreactor (Sponza and Agdag, 2004; Sormunen et al., 2008); however, there is no clear proof that the landfill will reach complete stabilization. In addition, the time period for this to occur is not known. To solve this problem, the physical and chemical processes occurring inside the landfill need to be well understood. A combination of different disciplines, like biogeochemistry, stochastic modeling, hydrogeoengineering, and geophysics, is required to develop a "user-friendly" methodology, which includes measurements and modeling, that can predict the emissions potential of a landfill (Bun et al., 2012; Heimovaara et al., 2012).

Geophysical exploration methods, like seismics and electrical resistivity, can be used to obtain an image of the subsurface; the image may provide information from which leachate flow paths may be deduced. In addition, quantitative mechanical values can be estimated that will show the density distribution inside the landfill, which is important for predictive modeling of landfill emissions. Understanding the heterogeneity of the landfill in depth and time is important for improving the treatment technology (Powrie and Beaven, 1999). Our hypothesis is that, by imaging the high-density waste areas (scatterers) we would obtain insight into possible preferential flow paths and to what extent leachate is recirculated homogeneously through the landfill. Time-lapse geophysics is valuable as well, because subsurface parameters changing in time give an indication to what extent the landfill is stabilized.

Manuscript received by the Editor 8 March 2013; revised manuscript received 30 July 2013; published online 7 October 2013.
[1]Delft University of Technology, Section of Geoengineering, Department of Geoscience and Engineering, Delft, Netherlands. E-mail: L.A.Konstantaki@tudelft.nl; T.J.Heimovaara@tudelft.nl.
[2]Delft University of Technology, Section of Applied Geophysics and Petrophysics, Department of Geoscience and Engineering, Delft, Netherlands. E-mail: D.S.Draganov@tudelft.nl; R.Ghose@tudelft.nl.

Geophysical exploration methods have already been used to address the above problems; however, resolution, artifacts, and uncertainty in the results are still a significant problem. Jolly et al. (2011) studied the applicability of the electrical resistivity method on landfills to detect fluid movement inside the landfill and concluded that, although changes in apparent resistivity can be related to the location of horizontal drains, there is a significant uncertainty to what can be related to the true processes and what to the inversion artifacts. In addition, Bernstone et al. (2000) showed that it was not possible to distinguish between different types of material using electrical resistivity mapping alone and that high uncertainty was present in the results. Nevertheless, a combination of electrical resistivity measurements and induced polarization (Leroux and Dahlin, 2010; Dahlin, 2012) has shown promising results, being able to distinguish between waste and geologic material. However, an advanced inversion method is required for the optimization of the results. Electrical resistivity and induced polarization are methods that can help to resolve the moisture in the landfill, yet the results are mainly qualitative.

Reflection and refraction seismics have been tested on landfills as well (Lanz et al., 1998; Green et al., 1999; Balia and Littarru, 2010), but until now they have shown high uncertainties. De Iaco et al. (2003) have illustrated that the result of a conventional reflection seismic survey (CRSS) at a landfill is extremely difficult to interpret because strong scattering events and strong lateral velocity variations can influence the interpretation of the reflections and the source-generated noise.

Our aim is to image the subsurface of landfills to obtain an indication of the possible flow pathways. We propose to use the strongly heterogeneous and scattering subsurface of the landfills to our advantage by applying seismic interferometry (SI) to the CRSS data. We investigate the imaging and time-lapse application potential of SI with modeling studies.

SI traditionally refers to the process of retrieving the Green's function between two receivers from the crosscorrelation of recordings at the receivers from sources (primary or secondary) that surround them. SI can be applied to recordings from ambient noise (Campillo and Paul, 2003; Shapiro, 2004; Draganov et al., 2007; Draganov et al., 2009) or from transient (controlled) sources (Schuster, 2001; Wapenaar, 2002; Schuster et al., 2004). For a complete retrieval of the Green's function, the sources should enclose the receivers, but when the receivers are at the earth's surface, transient or noise sources are needed only in the subsurface (Wapenaar and Fokkema, 2006). In exploration seismics, the source geometry is reversed: the sources are present at the surface, where they are actually not required. Nevertheless, using stationary-phase arguments, it can be shown that also sources at the earth's surface can be used to retrieve the desired parts of the Green's function (Halliday et al., 2007). For retrieval of reflections, sources must be present at the surface at the intersection of the continuation of the specular ray after the energy has reflected from the subsurface reflectors. In this manner, for all subsurface transient sources equivalent source positions at the surface can be found. This means that, to retrieve the desired reflection response, one has to correlate a primary reflection arrival at one of the receivers with its free-surface multiple at the second receiver (van Wijk, 2006). Nevertheless, when sources are present only at the surface, the so-called *one-sided illumination* occurs and nonphysical arrivals arise in the retrieved reflection response (Snieder et al., 2006; Draganov et al., 2012; King and Curtis, 2012); these arrivals could be even stronger than the retrieved physical ones. When sufficient seismic energy is backscattered from the subsurface, for example due to many scatterers, the one-sided illumination might be compensated (Wapenaar, 2006).

As mentioned above, landfills are notorious for having many scatterers, which makes the interpretation of the CRSS data very complicated. Obtaining an image of the landfill is a challenging task as the migration algorithms are based on the single-scattering approximation. This approximation breaks down already at the shallower scatterers making the imaging of the deeper scatterers nearly impossible. Obtaining at least a partial image of the deeper part of the landfill might only succeed in the presence of sufficiently larger number of sources and receivers. The latter condition, though, would make a CRSS prohibitively expensive for the landfill operators for the (partial) subsurface information it would deliver. On the other hand, for the application of SI, the scatterers in the subsurface are an advantage because they act as secondary (Huygens) sources that help to illuminate the receivers from below and could suppress, at least partly, the nonphysical arrivals. Retrieval of correct SI reflection responses could be advantageous because virtual sources are created at each receiver position. This results in increased number of sources and recorded traces — something that is essential for imaging such a heterogeneous subsurface with high resolution. For example, in our case the SI-retrieved traces are almost five times more in number than the originally recorded from the CRSS. The increased number of sources (and thereafter traces), provides us with greater illumination angles, i.e., we increase the chances of rays penetrating the subsurface to scatterers and then being recorded at the surface after single scattering, thus resulting in an improved image.

DESCRIPTION OF THE MODELING STUDIES

To investigate the imaging and time-lapse monitoring potential of SI for landfills, we use examples from numerically modeled data. The numerical data are obtained using a finite-difference code (Thorbecke and Draganov, 2011) in acoustic mode. The spatial sampling is 0.2 m and the time sampling to avoid grid dispersion is 0.00005 s. To minimize the effect of reflection from the boundaries of our model, we apply a taper of 120 points at the model's vertical and lower boundaries.

The velocity model used for the forward modeling of the reflection shot gathers over a landfill is shown in Figure 1. We use S-waves instead of P-waves because S-waves provide higher resolution in soft soils, their velocity is linked to the stiffness, and S-waves are more sensitive to changes in the soil type (Ghose and Goudswaard, 2004). To record S-waves, we use horizontal sources and horizontal particle-velocity receivers. This way, use of an acoustic modeling scheme is justified, just as if one would use SH sources and receivers in the field. The full model is 600 m long and 50 m deep to further suppress the recording of reflections from the model boundaries. The landfill itself, as shown in Figure 1, is 100 m wide and 25 m deep. The background velocity of the medium surrounding the landfill is 250 m/s and its density is 1900 kg/m^3. The background velocity inside the landfill corresponds to that of loose sand and organic material and has a vertical gradient that starts at 200 m/s at the surface and ends at 220 m/s at 25 m depth. The background density of the landfill has a gradient as well: 1900 kg/m^3 at the surface and 1920 kg/m^3 at 25 m. Inside the landfill, we have distributed 48 scatterers randomly. Their sizes vary between 0.5 and 1.8 m in height and 0.35 and 3.89 m in length. These scatterers represent waste material that is not present in the surrounding landfill material (land and organic material) and thus have different seismic properties. The materials are selected based on published literature of waste composition, as described in Table 1. The data in the table show the waste composition that is common in the different studies. Relying on these relative percentages, we create areas that include plastics, metals, and glass. Plastic has an S-wave velocity of 440 m/s, glass is 2960 m/s, and metal is 3111 m/s (Kaye and Laby, 1995). We use lower velocities for the glass and metal scattering bodies of 1000 and 1300 m/s, respectively, as we do not expect to find large solid parts of glass or metal material, but rather a mixed aggregate of those along with loose sand and/or organic material. For the same reason, the densities are chosen to be 919, 2000, and 2050 kg/m^3 for the plastic, glass, and metal, respectively. Transient Ricker-wavelet sources and the particle-velocity receivers are placed on the surface. The wavelet of the sources has a peak frequency of 60 Hz. The total recording time of the reflection response is 1.5 s. The goal is to use the modeled reflection responses to image the scatterers, so that we would identify possible pathways between the scatterers.

The first forward CRSS modeling is performed using split-spread geometry. For this geometry, we use five cables of 24 receivers each, a 0.5 m receiver spacing and a 2 m source spacing. The first shot is placed at 2 m to the left of the left-most receiver. When the source position reaches the 96th geophone position, all the geophones to the left of the source (i.e., the four receiver cables that have been passed by the source), are moved to the right at the end of the line (Figure 2a and 2b). A total of 72 common-source gathers are forward modeled, resulting in a recording of 8640 traces in total. The forward-modeled data are then preprocessed to mute the direct arrivals, which do not contain reflection information, and are then prestack depth-migrated using a one-way shot-profile migration scheme to obtain a CRSS image of the landfills. For the migration we use, unless otherwise stated, the exact landfill's background-velocity model. The migration is based on optimized space-frequency wavefield extrapolation operators (Thorbecke et al., 2004).

We apply SI to the preprocessed data (i.e., the CRSS data after the muting). For that, we resort the common-source gathers to common-receiver gathers. Then we choose a receiver position at which we want to retrieve a virtual source (a master receiver). We correlate the master common-receiver gather with other common-receiver gathers and with itself. The following step is summation over the common source positions. The different common-receiver gathers might have different number of sources in common, so before correlation and summation, from the two common-receiver gathers to be correlated, we extract only those traces that are recorded using the same sources. Furthermore, we normalize the summation result by the number of the summed correlated traces. Aiming to obtain reliable results, we choose to correlate only those common-receiver gathers that have at least 10 sources in common. The result of the application of SI is retrieved virtual common-source gathers for each of the receiver positions, retrieving in total 42,048 traces for the split-spread geometry. Each of the retrieved virtual common-source gathers is deconvolved for the wavelet of the virtual source to compensate for the broadening of the wavelet after applying crosscorrelation. If

Table 1. Waste composition of landfills based on studies.

Study	Plastic	Textile	Metal	Wood	Glass	Paper	Organics
Gomes et al. (2005)	37.4%	33.3%	10.2%	2.8%	2.8%	0.9%	0.1%
Vilar and Carvalho (2004)	17%	3%	5%	4%	2%	2%	12%
Beaven et al. (2005)	16.67%	3.86%	1.78%	3.78%	3.65%	9.60%	60.66%
Spokas et al. (2006)	9.5%	10.5%	—	—	18%	19.5%	18%

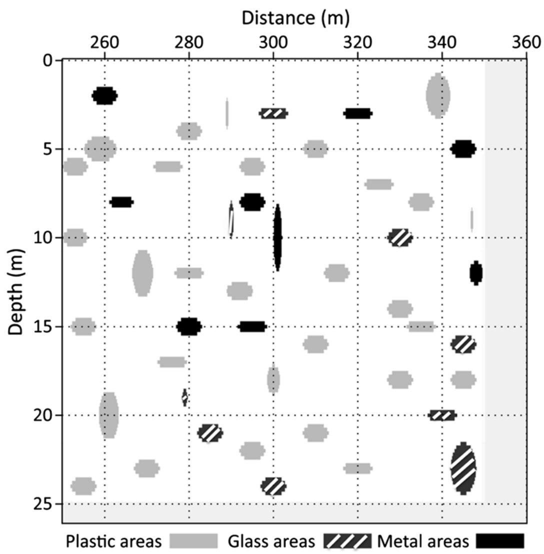

Figure 1. The velocity model used for the forward modeling. The shaded ellipses represent scatterers with different properties. The background velocity increases linearly from 200 m/s at the surface to 220 m/s at 25 m depth.

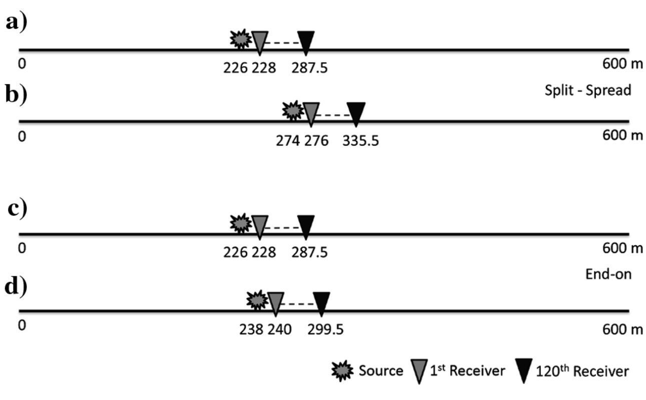

Figure 2. Split-spread geometry: (a) The geometry for the shot positions up to 272 m, then (b) the first 96 receivers are moved to the right, to the end of the first receiver (287.5 m) for shot positions 274–320 m and so on until the end of the line (383.5 m). End-on geometry: (c) The geometry for shot positions up to 236 m, then (d) the first 24 receivers are moved to the right, to the end of the last receiver (287.5 m) and so on until the end of the line (419.5 m). The pictures are illustrative and do not reflect the exact source-receiver placements.

the transient sources do not illuminate the receivers from all directions, parts of the desired reflections would be retrieved at positive times, but other parts at negative times. This would mean that one might need to sum parts of the retrieved positive and negative times to obtain a more complete retrieved reflection (for different cases of summation see, e.g., Draganov et al., 2009; Ruigrok et al., 2010). The presence of many scatterers in the subsurface helps to prevent such a situation, because the scatterers serve as secondary sources that help to illuminate the receiver array from below from many directions. Comparing the retrieved reflections at positive, negative, and sum times (not shown here) we observe that the retrieved results at positive times include the desired events, whereas the retrieved results at negative times include some undesirable correlation artifacts. We do, however, obtain migrated images for all three times separately and conclude that the positive times alone are sufficient to retrieve the desired reflections; therefore, we use only positive times. After that, we apply the same prestack depth migration as to the CRSS data. The obtained images are then top-muted to remove the imaging artifacts close to the surface due to correlation artifacts present in the retrieved virtual gathers at times earlier then the possible direct arrivals.

As a second forward-modeling geometry, we test the applicability of end-on acquisition. For this geometry, the first source and receiver positions and the source and receiver spacing are the same as that for the split-spread geometry. The total number of receivers (receiver cables) is also the same. However, here the receiver cables are moved more frequently. When the source position reaches the end of the first receiver cable (24th receiver position), the first cable is moved to the right end of the total line so that there are always at least 96 geophones to the right of the source (Figure 2c and 2d). A total of 72 common-source gathers are forward modeled amounting to a recording of 8640 traces.

In the following section, we examine the two acquisition geometries for their applicability to our purposes. We compare images for the case when: The exact migration velocity is known, we have an error in the migration velocity, there is source nonrepeatability error, and there is erroneous muting of the direct arrivals in the CRSS gathers.

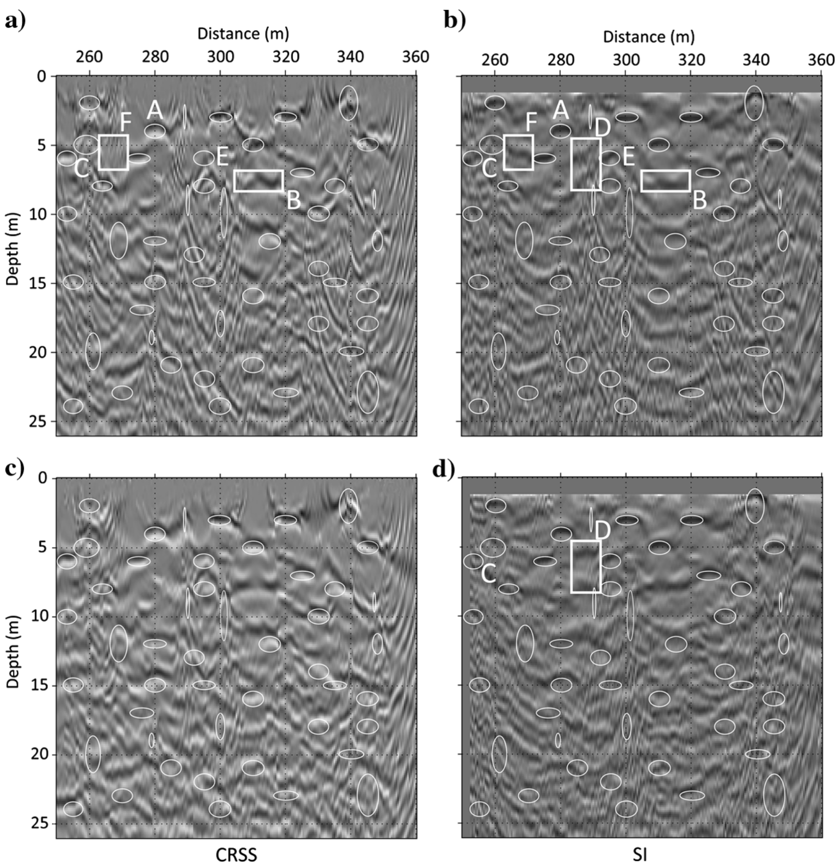

Figure 3. The prestack depth migrated results for (a) conventional reflection seismic survey (CRSS) using a split-spread geometry, (b) seismic interferometry (SI) applied to recordings from a split-spread geometry, (c) CRSS using an end-on geometry (d) SI applied to recordings from an end-on geometry. The white ellipses indicate the positions of the scatterers from the model in Figure 1. Automatic gain control with a window of 5 m is applied to the images. Ellipse A and E are examples of scatterers that are better resolved in the SI image; rectangle B encloses an example area inside which an artifact present in the CRSS image is suppressed in the SI image. The ellipse labelled C indicates a scatterer that is better imaged using the data from the CRSS; rectangle F shows an example of worse imaging in SI; rectangle D shows an area in the image that is better resolved in SI data when using recordings from split-spread geometry compared to end-on geometry.

RESULTS

Comparison of the images obtained from CRSS and SI data

Figure 3a and 3b shows the prestack depth-migrated results for CRSS and SI, respectively, with split-spread geometry. An automatic gain control with a 5-m window is applied to enhance the visualization of deeper reflections. In all figures, the white ellipses depict the position of the scatterers, as visible in Figure 1. Comparing the two images, we can see that the shallower scatterers are, in general, better-resolved in the SI image than in the CRSS image: The position of the focused energy is more precise and there are less imaging artifacts. For example, the ellipse A at the horizontal distance 280 and 4 m depth (280,4) is more compactly (and thus more precisely) focused in the SI image. The same holds for most of the shallow scatterers, e.g., at positions (300,3), (320,3), (339,2). To illustrate this, we plot the trace at distance 260 (trace 260) from the CRSS and SI images (Figure 4a and 4b) where the boundaries of the scatterers, intersected by this trace, are visualized by the gray rectangles. In the CRSS image, the shallowest scatterer is not imaged, possibly because the arrivals from this scatterer were partly muted during the muting of the first arrivals. In the SI trace; however, this scatterer is imaged even though part of the wavelet is missing due to the top mute applied after the migration. Due to the presence of multiple scattering, during the retrieval process, SI would retrieve a final arrival from a scatterer not only from the correlation of earlier arrivals in the CRSS recordings (which might be damaged by the muting), but also from the correlation of later arrivals in the CRSS recordings (which are unaffected by the muting). The scatterer around 5 m depth will be misinterpreted in the CRSS due to the strong event in the trace just between the positions of the two scatterers. Also in the SI image such a strong event is present, which makes the interpretation of the scatterer around 5 m here questionable. The strong events might be free-surface multiples of the shallowest event, which would mean that the event in the SI image at the position of the scatterer around 5 m might be a second-order free-surface multiple of the shallowest scatterer. The deepest scatterers in both traces are not unambiguously interpretable.

Due to the increased number of virtual sources in the SI data, some artifacts that are present in the CRSS image are suppressed in the SI image. Due to multiple scattering, the imaging algorithms, which are based on the single-scattering approximation, might focus multiple-scattered energy at erroneous places. This is illustrated by the white rectangle B in Figure 3a, where it appears that there is a scatterer, but at a wrong place. In the SI image, this erroneously focused energy is suppressed.

As mentioned in the introduction, the imaging of a highly scattering subsurface is a challenging task. Even though the shallow part of such a subsurface could be imaged, as we see from the above, the imaging of the deeper parts would most probably fail. This is essentially a limitation of the imaging algorithms, which are based on single-scattering approximation. The limitation of the imaging algorithms might be reduced to some extent by the utilization of denser source and receiver sampling. This, though, would make the CRSS prohibitively expensive for landfill operators for monitoring purposes of the total area of a landfill that can be quite large (e.g., 56 hectares in the case study of Gomes et al., 2005). For a landfill survey with a realistic geometry as used by us, the advantage of applying SI to the already recorded CRSS is shown above (Figures 3a, 3b, 4a, and 4b) for imaging the shallowest scatterers (until 5 m depth). In general, though, the images of both data sets fail to image scatterers below 15 m and also fail to image the bottom of the landfill at 25 m depth. However, SI shows improvement over CRSS in imaging some of the intermediate-depth scatterers, those between 5 and 15 m. For example, ellipse E (295,6) is imaged with the SI data and could now be interpreted as a scatterer, whereas using the CRSS image that would not be possible. Another example of better result in the SI image is the scatterer at (325,7). Nevertheless, the extra imaging powers of the SI data (due to additional illumination from more virtual sources) are limited by the imaging algorithms. As seen in Figure 3a and 3b, CRSS and SI image the scatterer at (280,15) at the wrong position. In this case, this is an imaging artifact due to the used migration velocity; which does not include the scatterers (the scatterers' velocity is higher than the background one). The reason why some deeper events are visible and some are not, is due to the fact that there are no direct rays to be scattered by the ellipses and be recorded at the surface without further scattering. SI images the scatterers relatively better because it provides more virtual sources, therefore more rays penetrate into the subsurface and are recorded after a single scattering.

Although, in general, SI provides a clearer and more interpretable result, some areas — the two vertical boundaries of the landfill — are better imaged with the CRSS data. For example, ellipse C (253,6) is better imaged with CRSS. This is because of the process of applying SI, which involves summation over sources. To obtain a reliable result from the application of SI to the CRSS data, we choose to sum correlated traces that have at least 10 sources in common. This means that for the beginning and the end of the survey line this condition is not met and there the SI data contain fewer traces than the original CRSS data. There are also places in the images where the SI image has performed worse than the CRSS image by focusing energy, which is not present in the CRSS image. Such an example is shown in the rectangle F in Figure 3a and 3b.

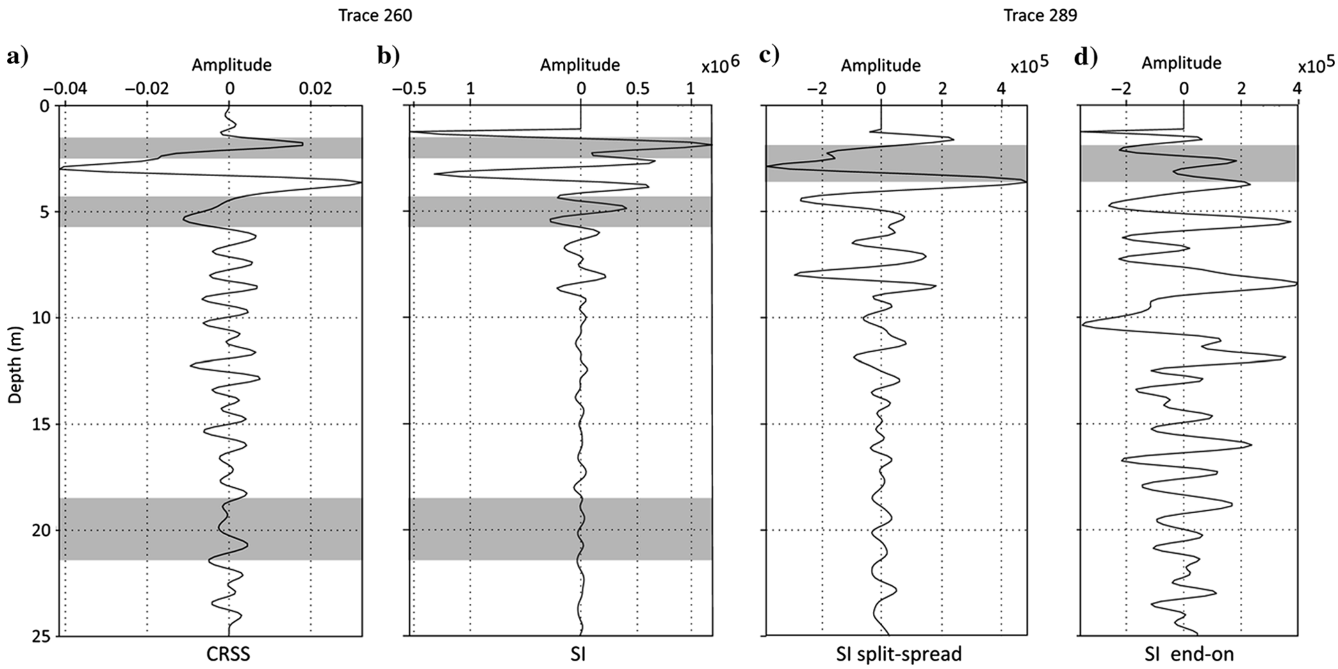

Figure 4. (a) Trace at horizontal distance 260 (trace 260) from the CRSS image with split-spread geometry. (b) Trace 260 from the SI image with split-spread geometry. (c) Trace 289 from the SI image with split-spread geometry. (d) Trace 289 from the SI image with end-on geometry. The gray rectangles represent the boundaries of scatterers that are intersected by these traces as shown in Figure 1.

Nevertheless, there are only a few such places and that does not counter the rest of the advantages of the SI image.

Beside spatially better spatial focusing of the focused energy, SI shows a relatively higher signal-to-noise ratio (S/N) with less artifacts than CRSS. As explained above, the extra traces in the SI data help suppress some artifacts. Others, like the event around position (310,17), could be mistaken for a scatterer and consequently have an influence on our interpretation. To illustrate the better S/N, we show in Figure 5a and 5b the same result as in Figure 3a and 3b but without an automatic gain control. We can appreciate in the SI image the overall reduction in focusing artifacts and thus the overall increase of the S/N.

Acquisition geometry: Split-spread or end-on

As already discussed, SI generally provides improved imaging versus CRSS for a heterogeneous environment like a landfill. The relative improvement would depend on the acquisition geometry used during the CRSS. Here, we compare influence of split-spread and end-on acquisition schemes on the image that can be obtained from the retrieved SI data, see Figure 3b and 3d, respectively. Comparing the SI end-on result (Figure 3d) with the SI split-spread result (Figure 3b), we can conclude that the split-spread geometry provides a better basis for obtaining an improved image. Event C that was discussed before, is nearly not interpretable in the end-on image. This happens because of the summation in the SI retrieval procedure. To obtain reliable results, we set a confidence level of 10 shots in common for the summation. Our acquisition geometry starts and finishes with active sources very close to the vertical boundaries of the landfill. Due to this, the confidence level for the split-spread geometry is reached for retrieved traces at receiver positions closer to the boundaries than for the end-on geometry. The possible fluid pathways that we want to interpret are also imaged differently, the white rectangle below ellipse D (289,3) shows a pathway that in the end-on image appears obstructed by imaging artifacts, but appears at least partly open in the image from the split-spread geometry. The imaging is worse in the end-on result as well. For example, ellipse D (289,3) is difficult to interpret in the end-on image, whereas it appears clearly in the split-spread image. Trace 289 in Figure 4c and 4d shows the differences in focused energy between the end-on and split-spread geometry and the worse S/N in the end-on result. The gray rectangle shows the position of scatterer D (289,3), which is imaged in the split-spread geometry result of the SI data (Figure 4c), but not in the end-on result of the SI data (Figure 4d). The advantage of split-spread geometry is that it moves the receiver cables less often, resulting in more continuous recording than with the end-on geometry. Having more continuity translates, in our case, to retrieving larger offsets and ultimately larger fold.

Influence of errors in the migration velocity

As is well known (Zhu et al., 1998), errors in the velocity model used for migration in the imaging algorithms would result in errors in the obtained images. For a subsurface layer, that would mean that the layer might be imaged at a wrong position. For a highly scattering media like a landfill, the problem would be exacerbated. All the images until now were obtained using the exact background velocity model (without the scatterers) used in our forward model. In real acquisition, however, the migration velocity will not be exactly known. It could be estimated from the direct arrivals or from the surface-wave analysis, but that would introduce uncertainties. For this reason, we test the effect a 25% error in the background velocity model would have on our results. Figure 6 depicts the results of imaging using the CRSS and SI data with error in the migration velocity for the split-spread geometry. The error in the migration velocity affects both images strongly, but the result is more adverse in the CRSS image. The energy that was focused

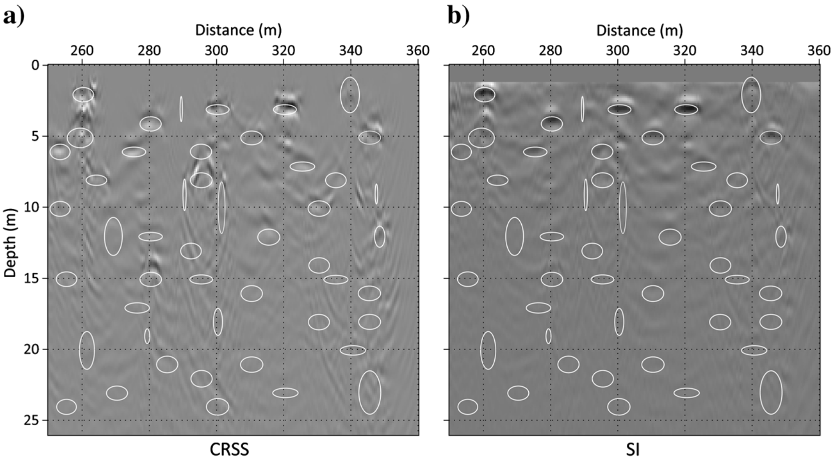

Figure 5. The prestack depth migrated images for split-spread geometry using (a) CRSS and (b) SI data without application of automatic gain control.

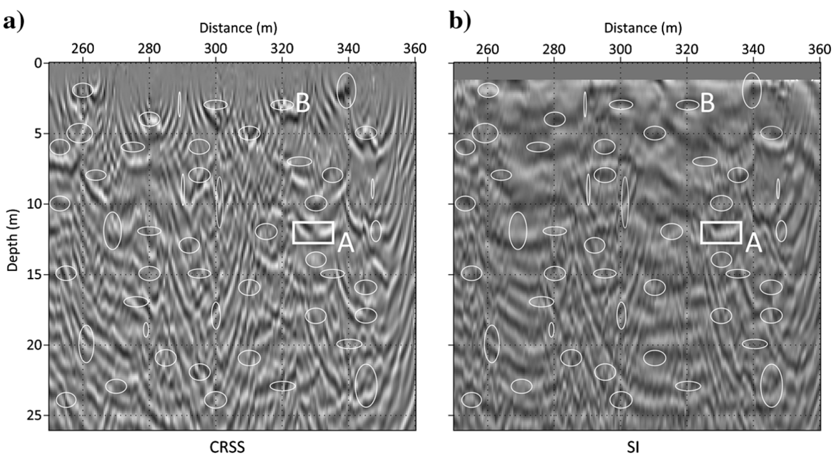

Figure 6. As in Figure 3a and 3b, but when the migration velocity has a 25% error. Ellipse B is an example of a relatively clearer imaged scatterer in the SI image, whereas rectangle A shows a zone of the image exhibiting a suppressed artifact in the SI image compared to the strong artifact in the CRSS image.

in the shallower part of the CRSS image using the exact background velocity (Figure 3a) is now smeared in migration smiles and renders the image too noisy to interpret the presence of possible scatterers (Figure 6a). The SI image in Figure 6b exhibits better focusing of the energy in the shallower part resulting in less overall noise and thus makes interpretation of scatterers possible, albeit at the incorrect place. The better S/N in the SI data could be appreciated comparing, for example, the imaging of the scatterer labeled B in Figure 6a and 6b. Also, in this case, the extra illumination of the subsurface in the SI data due to the extra virtual sources helps suppress strong artifacts present in the CRSS image (compare the area delineated by the white rectangle A in Figure 6a and 6b).

Time-lapse seismic monitoring

To monitor changes in the landfill with time, time-lapse seismics could be used. For this, a base survey could be recorded, for example, at an early time of the development of the landfill and a monitor survey at a later time. Changes in the positions of the scatterers that might have occurred between the two surveys could then be visualized, for example, by taking the difference of the depth images obtained for the base and the monitor surveys. A notorious problem during time-lapse seismics is the nonrepeatability of the positioning of the sources and the receivers. The later could be addressed by installation of permanent network of receivers. For landfill application this might be feasible, but solving the source nonrepeatability in such a way would be relatively expensive for landfill operators. For this reason, we model the monitor survey assuming exact repeatability in the receiver positioning, but errors in the positioning of the sources for a subsurface where no changes have occurred between the two surveys. Having no changes in the subsurface and in the receiver positions allows us to quantify the changes that occur due to the error in the source position between the two surveys. The source-positioning errors are modeled by introducing random errors in the horizontal position of each source from 0 to 1 m around its position in the base survey.

Comparing the images for the base survey (Figure 3a and 3b) and the monitor survey (Figure 7a and 7b) and their difference panels (Figure 7c and 7d) for the CRSS and SI data, we can see that the SI images and difference panels are largely unaffected by the source nonrepeatability. Nearly all the scatterers in the SI image from the monitor survey are imaged at the same position as in the base survey, but this is not the case for the CRSS images. This is visible also in Figure 8, where trace 320 in the images for the base and monitor surveys for the CRSS and the SI data are compared. The imaged traces from the SI data show much better wavelet reproducibility and far fewer differences compared to the traces from the CRSS data. This happens as SI redatums the erroneous source positions in the CRSS survey to virtual-source positions at the receiver locations, each of which is fixed for the base and monitor surveys. To quantify the effect of nonrepeatability on the images from the CRSS and SI data, we compute the normalized root mean square value (NRMS) (Mehta et al., 2007). The NRMS in our case is defined as

$$\mathrm{NRMS} = \sqrt{\frac{\langle (x2 - x1)^2 \rangle}{\left\langle \frac{x2^2 + x1^2}{2} \right\rangle}}, \tag{1}$$

where $x2$ is the energy at a given point in the image from the monitor survey and $x1$ — the energy at the same point but in the image from the base survey. The symbol $\langle\rangle$, in this case, represents the average over the value computed in the nominator and the denominator, respectively. We compute the NRMS for the whole area of the modeled landfill. The NRMS for the CRSS images is 84%, whereas for the images from the SI data it is 14%. The lower the percentage, the more repeatable the result, which quantifies the benefit of applying SI to CRSS landfill data for time-lapse purposes.

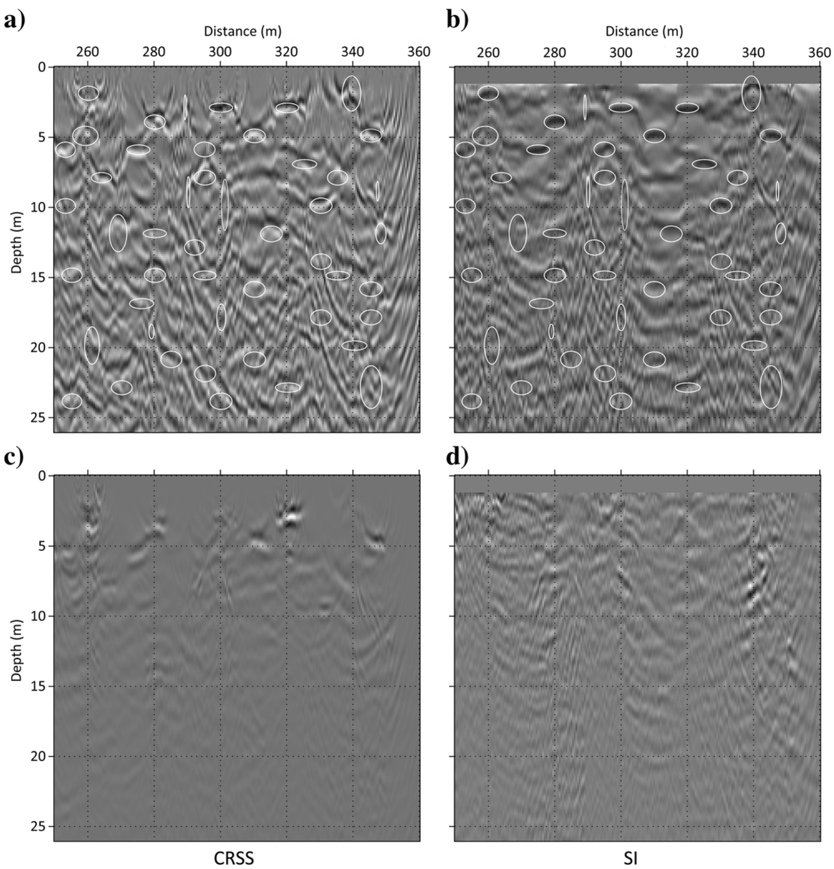

Figure 7. (a) Prestack depth migrated image from CRSS data with nonrepeatability errors in the source positions. (b) Prestack depth migrated image from SI data obtained from CRSS survey used in (a). (c) Difference panel between the image in (a) and the image in Figure 3a for the CRSS data. (d) Difference panel between the image in (b) and the image in Figure 3b for the SI data. The white ellipses show the position of the scatterers as shown in Figure 1. The images in (a and b) are visualized after application of automatic gain control with a window of 5 m.

Influence of muting the direct arrivals on imaging the shallow scatterers

An important processing step before obtaining an image is the muting of the direct arrivals (direct S- and surface waves). For field data, the best procedure would be to do the muting manually for each common-source panel. For large data sets, though, this could be time-consuming and thus automatic muting could be used instead. The latter might prove less optimal and result in eliminating diffractions (or depending on the size — reflections) from the shallowest scatterers, which would result in worse imaging. To test the effect of the automatic muting, we apply automatic muting on the data from the CRSS base survey, apply SI to these data, and then prestack depth migrate both data sets. The new images are subtracted from the respective images in Figure 3a and 3b. The difference panels are shown in Figure 9a and 9b. Comparing the two difference panels, we can see that the imaging of the shallow scatterers with the CRSS data can be erroneous due to suboptimal muting. Contrary to that, the image of the shallow scatterers obtained from the SI data is nearly unaffected. This is supported by the calculated NRMS values: 28% for SI and 82% for CRSS. As explained above, SI retrieves diffraction (or reflection) arrivals from the shallow scatterers using also multiple scattered energy and

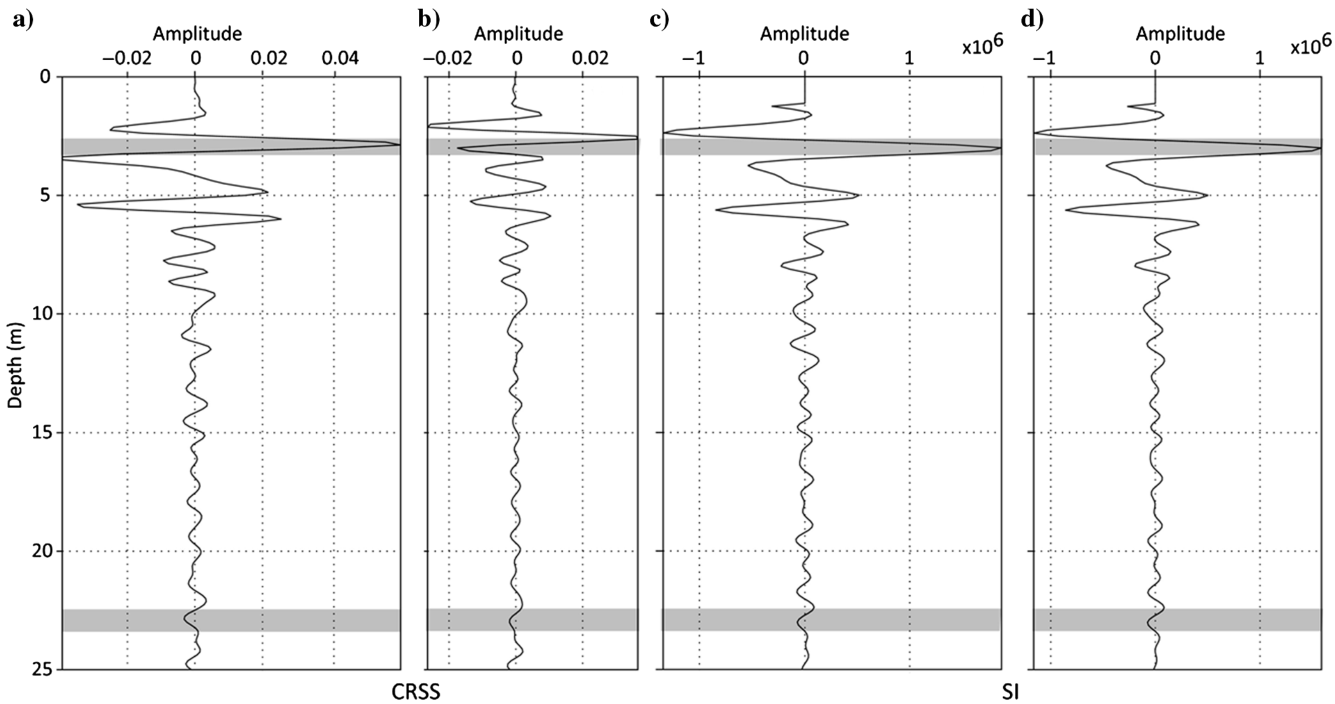

Figure 8. Trace 320 from the images obtained using data from (a) CRSS base survey, (b) CRSS monitor survey, (c) SI base survey, and (d) SI monitor survey. The gray rectangles represent the boundaries of scatterers from Figure 1 that are intersected by these traces.

Figure 9. (a) Difference panel between the survey with automatic muting and the image in Figure 3a for the CRSS data. (b) Difference panel between the survey with automatic muting and the image in Figure 3b for the SI data.

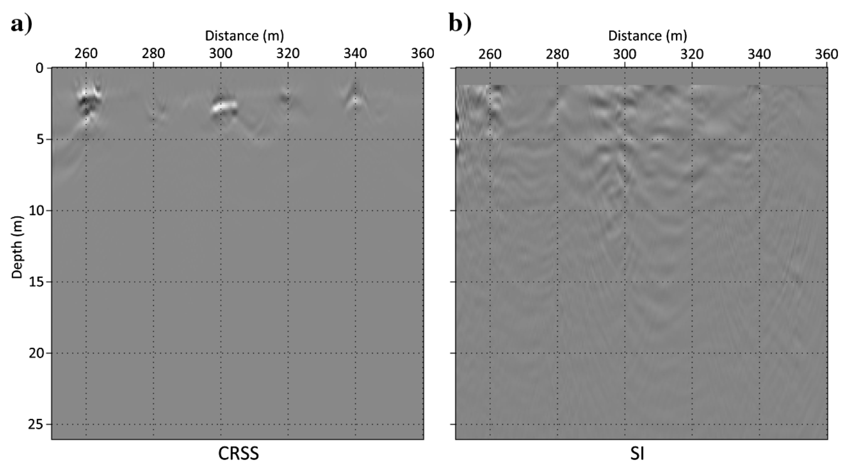

as a result is much less affected by erroneously muted arrivals from the shallow scatterers.

DISCUSSION

The goal of our modeling studies was to investigate whether the application of SI to data from CRSS acquired over a highly scattering subsurface, such as a landfill, could help improve the imaging of the subsurface. For the landfill, an accurate imaging of the scatterers is important to understand well the flow paths and the heterogeneity within the landfill. This, in turn, is needed for improvement of the treatment method for landfills. Our results show that for the tested acquisition geometries, data obtained from SI provide better images of the shallow scatterers in a landfill than the original CRSS data.

Nevertheless, obtaining an image of the deeper scatterers remains a challenge, as the CRSS and SI data provide an unambiguous image of these scatterers. To try to address this problem, we tested the results of application of SI with split-spread geometry to recordings with shorter receiver spacings: 0.25 and 0.10 m. We did this because having more receivers might result in improved subsurface images. The results, however, showed marginal improvement of the subsurface images, which might not justify use of denser, and thus more expensive, acquisition. Note that the difficulty in obtaining an image of the deeper part of the landfill lies in the migration algorithms, which are based on single-scattering approximation. To be able to image the deeper scatterers with a good resolution, a migration algorithm that accounts for multiple scattering should be used (Fleury and Vasconcelos, 2012; Vasconcelos et al., 2012; Ravasi and Curtis, 2013).

CONCLUSIONS

We investigated the application of SI to data from CRSS for obtaining information of a highly scattering subsurface like a landfill. Application of SI to CRSS data would normally retrieve a lot of nonphysical arrivals, but due to the multiple scattering in the landfill, the nonphysical arrivals in the SI data are suppressed. For the investigated acquisition geometries, we showed that the SI data can provide a better image of the landfill than the CRSS data. The image from the SI data exhibits less artifacts and the shallow scatterers are imaged with higher precision. We also showed that the image from the SI data is less sensitive to errors in the migration velocity and in the muting of the direct arrivals. For purposes of monitoring of possible changes in the location of the scatterers, and thus the flow paths in the landfill, it is important to have a repeatable survey. We showed that application of SI to the CRSS data suppresses the sources nonrepeatability errors and provides a very repeatable image.

ACKNOWLEDGMENTS

This research is supported by the Dutch Technology Foundation under the project number 11035. D. Draganov is supported by CATO2 and by the Division for Earth and Life Sciences with financial aid from the Netherlands Organization for Scientific Research.

REFERENCES

Balia, R., and B. Littarru, 2010, Geophysical experiments for the pre-reclamation assessment of industrial and municipal waste landfills: Journal of Geophysics and Engineering, **7**, 64–74, doi: 10.1088/1742-2132/7/1/006.

Beaven, R. P., L. Dolla, O. A. Oni, and N. D. Woodman, 2005, A laboratory scale saturated and unsaturated tracer test through waste: Presented at the International Workshop Hydro-Physico-Mechanics of Landfills, LIRIGM.

Bernstone, C., T. Dahlin, T. Ohlsson, and H. Hogland, 2000, DC-resistivity mapping of internal landfill structures: Two pre-excavation surveys: Environmental Geology, **39**, 360–371, doi: 10.1007/s002540050015.

Bun, A., T. J. Heimovaara, S. M. Baviskar, A. van Turnhout, and L. A. Konstantaki, 2012, Integrated modeling and up-scaling of landfill processes and heterogeneity using stochastic approach: 7th Intercontinental Landfill Research Symposium (ICLRS), 55–56.

Campillo, M., and A. Paul, 2003, Long-range correlations in the diffuse seismic coda: Science, **299**, 547–549, doi: 10.1126/science.1078551.

Dahlin, T., 2012, Application of resistivity-IP to mapping of groundwater contamination and buried waste: Geophysical Association of Ireland Seminar on Environmental Geophysics.

De Iaco, R., A. G. Green, H. R. Maurer, and H. Horstmeyer, 2003, A combined seismic reflection and refraction study of a landfill and its host sediments: Journal of Applied Geophysics, **52**, 139–156, doi: 10.1016/S0926-9851(02)00255-0.

Draganov, D., X. Campman, J. Thorbecke, A. Verdel, and K. Wapenaar, 2009, Reflection images from ambient seismic noise: Geophysics, **74**, no. 5, A63–A67, doi: 10.1190/1.3193529.

Draganov, D., K. Heller, and R. Ghose, 2012, Monitoring CO_2 storage using ghost reflections retrieved from seismic interferometry: International Journal of Greenhouse Gas Control, **11S**, S35–S46, doi: 10.1016/j.ijggc.2012.07.026.

Draganov, D., K. Wapenaar, W. Mulder, J. Singer, and A. Verdel, 2007, Retrieval of reflections from seismic background-noise measurements: Geophysical Research Letters, **34**, L04305, doi: 10.1029/2006GL028735.

Fleury, C., and I. Vasconcelos, 2012, Imaging condition for nonlinear scattering-based imaging: Estimate of power loss in scattering: Geophysics, **77**, no. 1, S1–S18, doi: 10.1190/geo2011-0135.1.

Ghose, R., and J. Goudswaard, 2004, Intergrating S-wave seismic reflection data and cone-penetration-test data using a multiangle multiscale approach: Geophysics, **69**, 440–459, doi: 10.1190/1.1707064.

Gomes, C., M. L. Lopes, and M. G. Lopes, 2005, A study of MSW properties of a Portuguese landfill: Presented at the International Workshop Hydro-Physico-Mechanics of Landfills, LIRIGM.

Green, A. G., E. Lanz, and H. Maurer, 1999, A template for geophysical investigations for small landfills: The Leading Edge, **18**, 248–254, doi: 10.1190/1.1438264.

Halliday, D. F., A. Curtis, J. O. A. Robertsson, and D.-J. van Manen, 2007, Interferometric surface-wave isolation and removal: Geophysics, **72**, no. 5, A69–A73, doi: 10.1190/1.2761967.

Heimovaara, T. J., A. Bun, A. van Turnhout, L. A. Konstantaki, and S. M. Baviskar, 2012, Is it possible to quantify emission potential from high resolution monitoring of leachate dynamics?: 7th Intercontinental Landfill Research Symposium (ICLRS), 77–78.

Jolly, J. M., R. D. Barker, and R. P. Beaven, 2011, Resolution of electrical imaging of fluid movement in landfills: Proceedings of the ICE — Waste and Resource Management, **164**, 79–96.

Kaye, G. W. C., and T. H. Laby, 1995, Tables of physical and chemical constants, 2.4.1: The speed and attenuation of sound: Kaye and Laby Online, Version 1.0 (2005), http://www.kayelaby.nlp.co.uk, accessed 1 June 2012.

King, S., and A. Curtis, 2012, Suppressing nonphysical reflections in Green's function estimates using source-receiver interferometry: Geophysics, **77**, no. 1, Q15–Q25, doi: 10.1190/geo2011-0300.1.

Lanz, E., H. Maurer, and A. G. Green, 1998, Refraction tomography over a buried waste disposal site: Geophysics, **63**, 1414–1433, doi: 10.1190/1.1444443.

Leroux, V., and T. Dahlin, 2010, Time-domain IP and resistivity sections measured at four landfills with different contents: Near Surface, 16th European Meeting of Environmental and Engineering Geophysics.

Mehta, K., J. Sheiman, R. Snieder, and R. Calvert, 2007, The virtual source method applied to Mars field OBC data for time-lapse monitoring: 77th Annual International Meeting, SEG, Expanded Abstracts, 2914–2918.

Powrie, W., and R. P. Beaven, 1999, Hydraulic properties of household waste and implications for landfills: Proceedings of the ICE — Geotechnical Engineering, **137**, 235–247.

Ravasi, M., and A. Curtis, 2013, Nonlinear scattering based imaging in elastic media: Theory, theorems and imaging conditions: Geophysics, **78**, no. 3, S137–S155, doi: 10.1190/geo2012-0286.1.

Ruigrok, E. X., D. Campman, D. Draganov, and K. Wapenaar, 2010, High-resolution lithospheric imaging with seismic interferometry: Geophysical Journal International, **183**, 339–357, doi: 10.1111/j.1365-246X.2010.04724.x.

Scharff, H., 2005, Ideas and intentions of the Dutch sustainable landfill research programme: Presented at the International Seminar and Workshop on sustainable landfilling.

Schuster, G. T., 2001, Theory of daylight interferometric imaging: Tutorial: 63rd Annual International Conference and Exhibition, EAGE, Extended Abstracts, A–32.

Schuster, G. T., J. Yu, J. Sheng, and J. Rickett, 2004, Interferometric/daylight seismic imaging: Geophysical Journal International, **157**, 838–852, doi: 10.1111/j.1365-246X.2004.02251.x.

Shapiro, N. M., and M. Campillo, 2004, Emergence of broadband Rayleigh waves from correlations of the ambient seismic noise: Geophysical Research Letters, **31**, doi: 10.1029/2004GL019491.

Snieder, R., K. Wapenaar, and K. Larner, 2006, Spurious multiples in seismic interferometry of primaries: Geophysics, **71**, no. 4, SI111–SI124, doi: 10.1190/1.2211507.

Sormunen, K., M. Ettala, and J. Rintala, 2008, Internal leachate quality in a municipal solid waste landfill: Vertical, horizontal and temporal variation and impacts of leachate recirculation: Journal of Hazardous Materials, **160**, 601–607, doi: 10.1016/j.jhazmat.2008.03.081.

Spokas, K., J. Bogner, J. P. Chanton, M. Morcet, C. Aran, C. Graff, Y. M. Golvan, and I. Hebe, 2006, Methane mass balance at three landfill sites: What is the efficiency of capture by gas collection systems?: Waste Management, **26**, 516–525, doi: 10.1016/j.wasman.2005.07.021.

Sponza, D. T., and O. N. Agdag, 2004, Impact of leachate recirculation and recirculation volume on stabilization of municipal solid wastes in simulated anaerobic bioreactors: Process Biochemistry, **39**, 2157–2165, doi: 10.1016/j.procbio.2003.11.012.

Thorbecke, J., K. Wapenaar, and G. Swinnen, 2004, Design of one-way wavefield extrapolation operators, using smooth functions in WLSQ optimization: Geophysics, **69**, 1037–1045, doi: 10.1190/1.1778246.

Thorbecke, J. W., and D. Draganov, 2011, Finite-difference modeling experiments for seismic interferometry: Geophysics, **76**, no. 6, H1–H18, doi: 10.1190/geo2010-0039.1.

Van Vossen, W. J., 2010, Sustainable landfilling in the Netherlands: Developments, methodologies and experiences Österreichische Wasser und Abfallwirtschaft, **62**, 141–148.

van Wijk, K., 2006, On estimating the impulse response between receivers in a controlled ultrasonic experiment: Geophysics, **71**, no. 4, SI79–SI84, doi: 10.1190/1.2215360.

Vasconcelos, I., J. Robertsson, M. Vassallo, and D.-J. van Manen, 2012, Reverse-time imaging of dual-source 4C marine seismic data using primaries, ghosts and multiples: 74th Annual Conference and Exhibition, EAGE, Extended Abstracts, X045.

Vilar, O. M., and M. Carvalho, 2004, Mechanical properties of municipal solid waste: Journal of Testing and Evaluation, **32**, 12.

Wapenaar, K., 2006, Green's function retrieval by cross-correlation in case of one-sided illumination: Geophysical Research Letters, **33**, L19304, doi: 10.1029/2006GL027747.

Wapenaar, K., D. Draganov, J. W. Thorbecke, and J. T. Fokkema, 2002, Theory of acoustic daylight imaging revisited: 72nd Annual International Meeting, SEG, Expanded Abstracts, 2269–2272.

Wapenaar, K., and J. Fokkema, 2006, Green's function representations for seismic interferometry: Geophysics, **71**, no. 4, SI33–SI46, doi: 10.1190/1.2213955.

Zhu, J., L. R. Lines, and S. H. Gray, 1998, Smiles and frowns in migration/velocity analysis: Geophysics, **63**, 1200–1209, doi: 10.1190/1.1444420.